Lithos xxx (2013) xxx–xxx

Contents lists available at SciVerse ScienceDirect

Lithos

journal homepage: www.elsevier.com/locate/lithos

Origins of ultramafic rocks in the Sulu Ultrahigh-pressure Terrane, Eastern China

Zhipeng Xie [a], Keiko Hattori [b], Jian Wang [a,*]

[a] College of Earth Sciences, Jilin University, Changchun, Jilin, 130061, PR China
[b] Department of Earth Sciences, University of Ottawa, Ottawa, Canada K1N 6N5

ARTICLE INFO

Article history:
Received 5 September 2012
Accepted 10 December 2012
Available online xxxx

Keywords:
Sulu ultrahigh-pressure terrane
Subduction channel
Subcontinental lithospheric mantle
Forearc mantle serpentinite
Dunite
PGE

ABSTRACT

Ultramafic rocks in the Sulu belt are associated with high-pressure (HP) and ultra-high-pressure (UHP) rocks, a metamorphic product of the northern margin of the Yangtze Craton (YZC). These ultramafic rocks are important because they provide information relevant to the nature and evolution of the Mesozoic collisional belt. We selected ultramafic rocks from Yangkou Bay (YKB), Suoluoshu (SLS) and Hujialin (HJL) in the central region of Sulu belt. The ultramafic rocks in YKB and SLS are hydrated to form serpentinites and they contain low concentrations of moderately incompatible elements (Al, Ti, and V), high contents of Ir-group platinum-group elements (IPGE; Ir, Os, and Ru; 12.8–21.7 ppb in total), and high ratios (1.2–5.5) of IPGE to Pd-group PGE (PPGE) in bulk rocks. Spinel contains high Cr (Cr# = atomic ratio of Cr/[Cr + Al], 0.57–0.79). The data suggest that they likely represent hydrated forearc mantle peridotites underlying the margin of the North China Craton (NCC). Dunite samples from HJL are not fully hydrated with loss on ignition (LOI) values ranging from 6.6 to 13.2 wt.%, and contain olivine grains with high forsterite components (Fo = 100*Mg/[Mg + Fe], 91.7–92.4) and NiO contents (0.36–0.41 wt.%). Spinel grains show high Cr# (0.68–0.76). The bulk rock contains high IPGE (5.0–22.7 ppb total) and show high ratios (up to 8.8) of IPGE to PPGE. The data suggest that they are also residual mantle peridotites after high degrees of influx partial melting in the subduction setting. The geochemical features of our serpentinite and dunite samples are different from peridotites of young Cenozoic subcontinental lithospheric mantle (SCLM) that have been brought to the surface as xenoliths of young volcanic rocks. Instead, our samples are similar but even more refractory than peridotites of relict Archean SCLM below the NCC that were enclosed as xenoliths in Paleozoic–Mesozoic igneous rocks. Thus, the studied ultramafic rocks likely represent the relic of old refractory lithospheric mantle peridotites that underwent partial melting in the margin of the NCC during the subduction of oceanic lithosphere before the collision with the YZC. The peridotites in the forearc mantle were dragged into the subduction channel during the Mesozoic subduction of the YZC below the NCC, and exhumed together with the buoyant granitic metamorphic rocks in the Sulu belt.

1. Introduction

The Dabie–Sulu belt formed during the collision of the North China Craton (NCC) with the Yangtze Craton (YZC) followed by the subduction of the latter in Mesozoic time. The terrane is the largest and longest continuous ultrahigh-pressure metamorphic (UHP) belt in the world (Yang et al., 2003). The terrane contains volumetrically minor ultramafic rocks that form massifs and large lenticular bodies closely associated with UHP rocks (e.g., Zhang et al., 2000). These ultramafic rocks are mostly hydrated to form serpentinites, but some are relatively anhydrous, such as garnet peridotites, pyroxenites and dunites.

Proposed origins of peridotitic rocks in the Dabie–Sulu belt include 1) fragments of mantle wedge that have been incorporated into the YZC lithosphere during the subduction, 2) crustal cumulates that once belonged to the YZC before the subduction, and 3) protruded mantle peridotites that are not affected by later processes of subduction and UHP metamorphism (Zhang et al., 2000, 2009). The first type, fragments of mantle-wedge peridotites, is proposed for several ultramafic rocks in the Sulu belt based on major and minor element compositions. The examples include the Zhimafang ultramafic bodies reported by Zhang et al. (2008). The second type, crustal-cumulates, is reported for large ultramafic bodies in the Dabie belt. Good examples are the Bixiling and Maowu mafic–ultramafic complexes in the Dabie belt reported by Zheng et al. (2008). The third type is ultramafic complexes, which are mostly composed of spinel harzburgite and dunite, in the Raobazhai area of the northern Dabie belt (e.g., Zhang et al., 2009).

To evaluate the origin of ultramafic rocks and the evolution of the Sulu belt, we examined serpentinite and dunite bodies in three locations in the belt. This paper presents major- and trace-element compositions of bulk rocks and mineral chemistries of serpentinites from the Yangkou Bay (YKB) and Suouluoshu area (SLS), and dunites from the Hujialin area (HJL). The data are used to evaluate (1) the origins and protoliths of these ultramafic rocks, (2) the genetic relationship between hydrated and anhydrous rocks, and (3) the implications of the occurrences of these highly refractory peridotites in the Sulu belt.

* Corresponding author.
E-mail address: wangjian304@jlu.edu.cn (J. Wang).

0024-4937/$ – see front matter © 2012 Elsevier B.V. All rights reserved.
http://dx.doi.org/10.1016/j.lithos.2012.12.003

2. Geological setting

The Sulu UHP belt represents the eastern half of the Dabie–Sulu UHP terrane. The terrane formed during the Triassic subduction of the margin of the YZC beneath the NCC following the collision of the two continents. The rocks of the Sulu belt are well exposed in the southeastern part of the Shandong Peninsula, and the belt is bounded by the Tan–Lu fault and the Yantai–Wulian fault to the eastern NCC and the Jiashan–Xiangshui fault to the southeast (Fig. 1A). Rocks in the belt are mostly granitic orthogneisses and eclogites. U–Pb ages and Hf- and O-isotope data of zircon suggest that the majority of the gneisses have middle Neoproterozoic protoliths (780–740 Ma; Tang et al., 2008; Zheng et al., 2004). The gneisses and eclogites, along with garnet-bearing ultramafic rocks, were metamorphosed at 220–240 Ma (Gao et al., 2004; Liu et al., 2004, 2008; Yang et al., 2003; Zhang et al., 2005), reaching the peak condition of >5.0 GPa and >750 °C (e.g., Yang and Jahn, 2000; Zhang and Liou, 2003; Zhang et al., 2010). The presence of exsolved clinopyroxene, rutile and apatite in garnet from Yangkou eclogites attests that these eclogites were subducted to a depth greater than ~200 km (Ye et al., 2000).

We selected ultramafic rocks in the YKB and SLS–HJL areas because they are well exposed and spatially associated with HP–UHP rocks (granitic orthogneiss, paragneiss, eclogites) in the central region of Sulu belt. The YKB area is in the north-central Sulu belt, and the SLS–HJL areas are in the south-central portion of the Sulu belt (Fig. 1A).

The Yangkou ultramafic complex, near the city of Qingdao, is exposed as several bodies, tens of meters across, enclosed within granitic orthogneisses. The ultramafic complex consists mainly of garnet-bearing peridotites and serpentinites, and they display fine foliation from outcrop to thin-section scales (Wallis et al., 1997). Mineralogical and petrological studies by Yoshida et al. (2004) suggested that the garnet peridotites were originally mantle peridotites and have undergone a UHP metamorphism together with the surrounding orthogneisses. Since serpentinites have sharp boundary with anhydrous garnet peridotites, the two may have different origins and evolution histories.

The SLS and HJL ultramafic rocks occur near the town of Rizhao. They form lenticular bodies ranging from tens of meters to several kilometers in size. The long axes of the ultramafic bodies are parallel to the regional gneissosity of surrounding granitic orthogneisses. They are considered to be rootless and have tectonic contacts with the surrounding gneisses (e.g., Gao et al., 2004; Yang, 2006). The SLS body is a large lens (the length > 6 km) in the direction of NNW–SSE (Fig. 1C), and mostly composed of serpentinites and minor pyroxenites. The HJL body is about 6 km long, strikes NNW to SSE and bent to EW at its north end (Fig. 1C), and it consists of serpentinites with minor discontinuous lenses of garnet clinopyroxenite and dunite (Yang, 2006; Zhang and Liou, 2003). The studied dunite lenses show sharp contacts with the surrounding serpentinites. Zircon in garnet clinopyroxenites gave U–Pb ages of ~216 Ma (Gao et al., 2004), which are interpreted to be the age of metamorphism.

3. Petrology of ultramafic rocks

Samples collected from YKB, SLS, and HJL are all representative rocks of the ultramafic bodies, and they were carefully selected after field examination of outcrops. We examined a total of ten samples including serpentinite from YKB (YKB1, YKB2, YKB3) and SLS (SLS1,

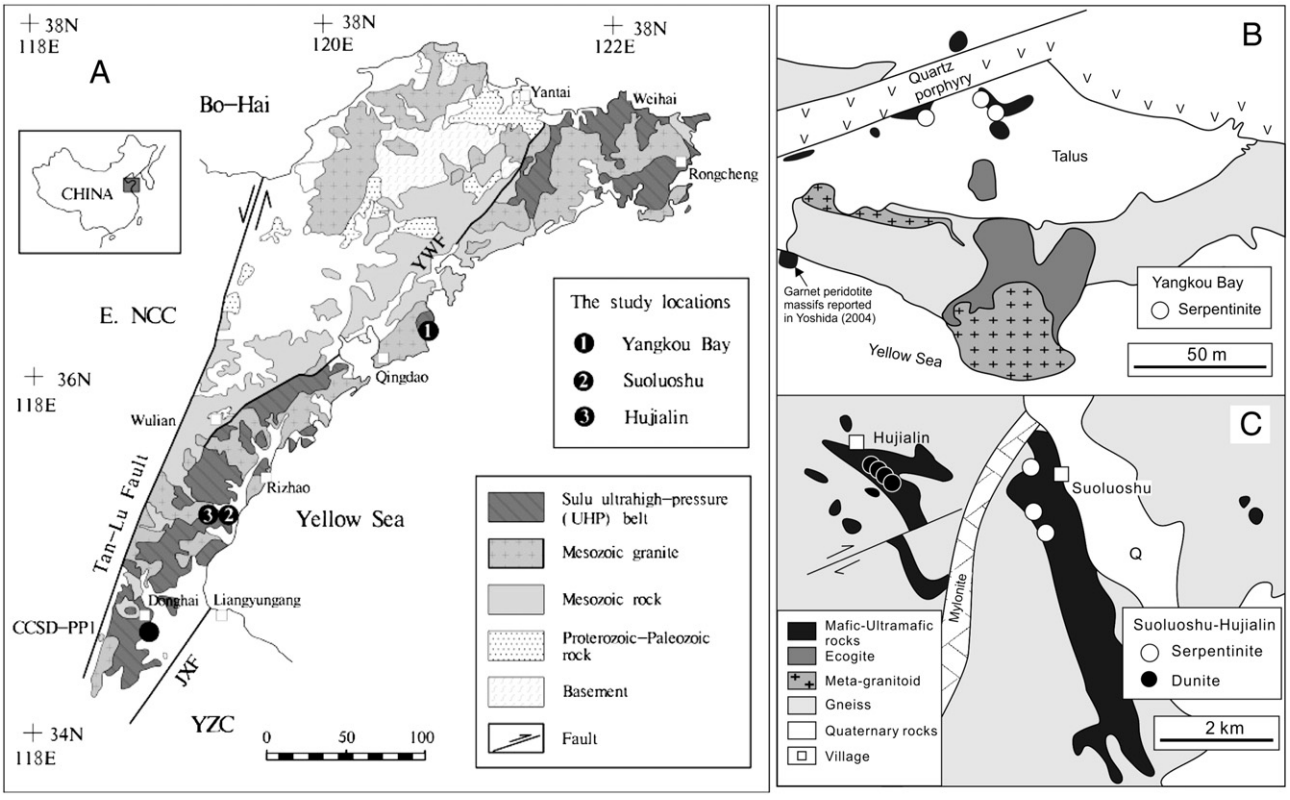

Fig. 1. (A) The regional map showing the distribution of the Sulu ultrahigh pressure terrane (dark grey), Mesozoic granitic intrusions (cross marked area), Proterozoic–Paleozoic rocks (dotted area) and Archean basement rocks (lightly dotted area) (modified after Yao et al., 2000). The Sulu belt is bounded by Yantai–Wulian fault (YWF) and Tan-Lu fault to the west and Jiashan-Xiangshui fault (JXF) to the southeast. The locations of the study areas are shown with solid circles; 1 = Yangkou Bay, 2 = Suouluoshu, and 3 = Hujialin. (B) Simplified geology of the Yangkou Bay area showing the distribution of ultramafic bodies (solid) (modified from Wallis et al., 1997) with locations of 3 serpentinites samples; (C) Simplified geology of the Suoluoshu-Hujialin area showing the distribution of mafic-ultramafic complexes (modified from Gao et al., 2004), with locations of 3 serpentinite and 4 dunite samples. The villages of Hujialin and Sholuoshu are shown with open squares.

Please cite this article as: Xie, Z., et al., Origins of ultramafic rocks in the Sulu Ultrahigh-pressure Terrane, Eastern China, Lithos (2013), http://dx.doi.org/10.1016/j.lithos.2012.12.003

SLS2, SLS3), and dunite from HJL (HJL1, HJL2, HJL3, HJL4). Their outcrop locations are shown on Fig. 1B and C.

Serpentinites from YKB are completely hydrated with high loss on ignition (LOI, 12.8–15.0 wt.%; Table 1). They are collected within the northern part of the ultramafic bodies (Fig. 1B). Samples are dark gray and show equigranular (0.3–0.8 mm) texture in hand specimens. Mineral assemblages of samples YKB3 and YKB5 are mainly serpentine (subhedral, 0.3–0.8 mm, 60–80 vol.%), talc (fine-grained aggregate, 10–30 vol.%), clinochlore (blades, 0.3–0.5 mm, ≤5 vol.%), chromite (0.1–0.3 mm, ≤5 vol.%), and minor brucite, whereas sample YKB4 is mainly composed of talc (70 vol.%), clinochlore (15 vol.%), chromite (<5 vol.%), and minor serpentine (<10 vol.%) (Table 2; Fig. 2A, C, D). Serpentine grains in sample YKB3 and YKB5 are pseudomorphic, retaining the shape of original olivine and orthopyroxene grains (Fig. 2A, C; Table 2), and they are commonly surrounded by radial aggregates of talc. The pseudomorphic texture of serpentine suggests that the primary mineralogy is olivine (≤85 vol.%) and orthopyroxene (≥15 vol.%) and their protolith is most likely harzburgite.

Serpentinites from SLS were also completely hydrated with high LOI (15.8–17.7 wt.%; Table 1). They are dark green-gray, intensely foliated, and show equigranular (0.2–0.5 mm) texture. Samples from SLS are mainly composed of serpentine (subhedral, 0.2–0.5 mm, 60–80 vol.%), talc (10–20 vol.%), chromite (0.1–0.3 mm, ≤5 vol.%), and minor chlorite and brucite (Fig. 2B; Table 2). Serpentine is pseudomorphic with hourglass texture, retaining the shape of original grains of olivine and minor (<10 vol.%) orthopyroxene (Fig. 2B). The pseudomorphic grains of serpentine are rimmed by talc. The mineral texture suggests that their protoliths are most likely orthopyroxene-bearing dunite. Sample SLS2 contains late calcite veins, resulting in high CaO (1.69 wt.%) in bulk rock composition compared to other serpentinite samples (Table 1).

Dunite samples from HJL were partially hydrated to show LOI ranging from 6.6 to 13.2 wt.% (Table 1). The samples are greyish

Table 1
Bulk-rock chemical compositions of Serpentinites and Dunites from the Sulu belt, China.

Lithology	Analysis methods[c]	Serpentinite						Dunite			
Location		Yangkou Bay			Suoluoshu			Hujialin			
Samples		YKB3	YKB4	YKB5	SLS1	SLS2	SLS3	HJL1	HJL2	HJL3	HJL4
Major elements (wt.%)											
SiO_2	XRF	40.82	40.66	38.99	38.76	37.71	39.69	40.20	41.36	36.85	38.42
TiO_2	XRF	0.05	0.06	0.03	0.02	0.02	0.03	0.02	0.03	0.03	0.03
Al_2O_3	XRF	2.10	1.87	1.57	0.56	0.62	0.68	0.28	0.40	0.34	0.30
$Fe_2O_3(t)$[a]	XRF	5.13	7.00	6.87	6.06	5.85	6.00	7.09	6.81	8.69	7.59
MnO	XRF	0.09	0.10	0.11	0.10	0.09	0.07	0.11	0.11	0.13	0.12
MgO	XRF	39.24	38.41	37.54	40.37	38.55	39.15	45.41	44.68	40.84	46.17
CaO	XRF	0.10	0.19	0.09	0.08	1.69	0.21	0.48	0.47	0.85	0.43
Na_2O	XRF	<0.005	<0.005	<0.005	<0.005	<0.005	<0.005	<0.005	<0.005	<0.005	<0.005
K_2O	XRF	0.01	0.01	0.00	0.01	<0.005	<0.005	<0.005	0.01	<0.005	0.01
P_2O_5	XRF	0.01	0.01	0.01	0.01	0.01	0.01	0.01	0.01	0.01	0.01
LOI		15.01	12.83	14.74	15.82	17.74	17.22	6.95	8.20	13.21	6.60
Total		102.56	101.15	99.95	101.78	102.28	103.05	100.55	102.07	100.95	99.68
$Mg^{\#}$[b]		93.2	90.7	90.7	92.2	92.2	92.1	91.9	92.1	89.3	91.6
Trace elements in ppm											
Cr	XRF	2659	2532	2542	2412	2320	2863	2354	2478	5809	2790
Ni	XRF	2013	2532	1578	2175	2010	1942	2551	1982	2348	2643
Co	XRF	84	98	97	101	96	79	113	108	127	117
V	XRF	50	41	45	17	27	24	14	12	30	11
Cu	ICP–OES	0.9	40.7	0.9	2.1	0.52	0.39	1.38	0.99	3.7	0.62
S	ICP–OES	51.6	171	68.0	306	240	310	19.8	37.5	64.5	54.9
Pb	ICP–MS	10.1	3.0	7.1	7.7	0.3	6.1	0.6	0.8	1.8	0.5
Platinum-group elements in ppb											
Os	ID ICP-MS	4.7	3.9	3.9	5.2	7.3	5.7	4.7	5.7	7.8	1.1
Ir	ID ICP-MS	5.4	3.3	2.8	3.0	4.9	8.4	2.4	2.9	3.6	1.7
Ru	ID ICP-MS	6.7	6.1	6.1	7.5	9.5	7.3	6.7	6.4	11.2	2.1
Pt	ID ICP-MS	5.9	5.8	6.4	2.0	3.9	3.7	1.2	2.0	5.9	0.5
Pd	ID ICP-MS	3.6	5.3	3.7	0.8	0.5	0.3	0.4	0.8	6.7	0.6
Os + Ir + Ru		16.7	13.3	12.8	15.7	21.7	21.4	13.7	15.0	22.7	5.0
Pt + Pd		9.5	11.2	10.0	2.8	4.4	4.0	1.6	2.8	12.6	1.1
Ir/(Pt + Pd)		0.6	0.3	0.3	1.0	1.1	2.1	1.5	1.0	0.3	1.6
IPGE/PPGE		1.8	1.2	1.3	5.5	4.9	5.3	8.8	5.3	1.8	4.4
PGE-total		26.2	24.5	22.8	18.5	26.1	25.4	15.2	17.8	35.2	6.1

PGE reference	Os	Ir	Ru	Pt	Pd
TDB-1					
Recommended values[d]	0.12	0.08	0.18	5.01	24.30
This work ($n=5$)[e]	0.12 ± 0.016	0.11 ± 0.006	0.21 ± 0.045	4.59 ± 0.082	26.56 ± 0.002
JP-1					
Recommended values[d]	3.78	2.47	5.29	5.09	1.63
This work ($n=5$)[e]	4.26 ± 0.172	2.91 ± 0.167	6.27 ± 0.113	4.07 ± 0.395	1.60 ± 0.045

[a] Total Fe was expressed as $Fe_2O_3(t)$.
[b] $Mg^{\#}$ = atomic ratio of Mg*100/[Mg + Fe_{total}] in bulk rock.
[c] XRF, Philips PW-2400 X-ray fluorescence spectrometer; ICP-OES, VISTA-PRO inductively coupled plasma-optical emission spectrometer; ID ICP-MS, isotopic dilution inductively coupled plasma mass spectrometer.
[d] Average values obained by Meisel and Moser (2004).
[e] Number of analytical runs.

Please cite this article as: Xie, Z., et al., Origins of ultramafic rocks in the Sulu Ultrahigh-pressure Terrane, Eastern China, Lithos (2013), http://dx.doi.org/10.1016/j.lithos.2012.12.003

Table 2
Compositions of representative silicate minerals from serpentinites.

Sample:	YKB3			YKB4		YKB5			SLS1		SLS2	SLS3
Position:	Serp1	Serp2	Clc	Serp1	Clc	Serp1	Serp2	Clc	Serp1	Cch	Serp1	Serp1
SiO_2	43.24	38.29	31.25	44.00	32.31	42.50	38.63	32.06	46.15	35.42	45.70	45.01
Al_2O_3	0.39	6.27	17.55	0.26	14.32	0.89	5.32	14.13	0.13	9.86	0.12	0.08
FeO	1.05	2.86	3.00	2.23	3.54	1.36	3.26	3.46	0.95	5.30	2.07	1.82
MnO	0.00	0.07	0.00	0.04	0.00	0.03	0.04	0.00	0.01	0.04	0.04	0.03
MgO	40.84	36.06	32.65	38.87	33.22	40.12	36.78	32.76	41.81	35.24	39.90	40.35
CaO	0.04	0.09	0.02	0.04	0.03	0.03	0.03	0.00	0.01	0.03	0.03	0.04
Sum	85.56	83.64	84.47	85.44	83.42	84.93	84.06	82.41	89.06	85.89	87.86	87.33
O = 7												
Si^{4+}	2.03	1.86	1.51	2.08	1.59	2.02	1.87	1.59	2.08	1.71	2.09	2.07
Al^{3+}	0.02	0.36	1.00	0.01	0.83	0.05	0.30	0.83	0.01	0.56	0.01	0.01
Fe^{2+}	0.04	0.12	0.12	0.09	0.15	0.05	0.13	0.14	0.04	0.21	0.08	0.07
Mn^{2+}	0.00	0.00	0.00	0.00	0.00	0.00	0.00	0.00	0.00	0.00	0.00	0.00
Mg^{2+}	2.86	2.61	2.35	2.73	2.43	2.84	2.66	2.43	2.80	2.53	2.72	2.77
Ca^{2+}	0.00	0.00	0.00	0.00	0.00	0.00	0.00	0.00	0.00	0.00	0.00	0.00
Sum	4.96	4.96	4.99	4.92	5.00	4.96	4.97	4.99	4.92	5.01	4.90	4.92

Note: Serp—serpentine; Clc—Clinochlore; Serp1—the serpentine of serpentinized olivine; Serp2-the serpentine of serpentinized orthopyroxene.

grass yellow and show porphyroclastic or equigranular texture. Dunite is composed of fine–grained olivine (0.5–1.0 mm; 70–80 vol.%), serpentine (aggregate, ≤20 vol.%), and chromite (anhedral to subhedral; 0.2–1.0 mm; ≤5 vol.%). Olivine grains are subhedral and essentially free of any inclusions. Their rims are altered to a mixture of serpentine and minor magnetite (Fig. 2E).

In our ultramafic rocks including dunite, magnetite occurs disseminated in serpentine and rims chromite grains (Fig. 2A, B, D, E, G, H). Sulphide minerals in samples are fine–grained and granular (≤0.02 mm), and mostly pentlandite and some contain minor pyrrhotite (Fig. 2F, G). Serpentinite samples contain relatively high S (52–310 ppm), and most of sulphide minerals occur in the margins of aggregates of serpentine grains, suggesting that sulphur was likely introduced during the serpentinization. Sulphide minerals in dunite occur mostly in close association with serpentine along the grain boundaries of olivine, which also suggests late introduction of sulphur during the hydration of dunite. Rare inclusions of small (less than 10 μm) rounded grains of sulphide are found enclosed in olivine in dunites.

4. Analytical methods

Mineral compositions were determined using a CAMEBAX MBX electron probe in the wavelength dispersive method at the Carlton University in Ottawa. Counting times were 20s per element, and analytical conditions were 15 kV accelerating voltage, 20 nA beam current. The calibration used wollastonite (Si, Ca), synthetic spinel (Al), synthetic Cr_2O_3 (Cr), forsterite (Mg), synthetic $MnTiO_3$ (Mn, Ti), vanadium metal (V), albite (Na), fayalite (Fe in silicates), and synthetic Fe_2O_3. Fe^{3+} contents of spinel were calculated assuming a stoichiometric composition. Compositions of individual minerals are similar within individual samples, and representative compositions of minerals are listed in Tables 2–4.

The surfaces of our samples are weakly weathered, and these weathered portions were removed before bulk–rock geochemical analysis. The major element compositions of bulk rock samples were analyzed with a Phillips PW 2400 X–ray fluorescent spectrometer after fusing bulk–rock powder with a flux composed of 78.5% $Li_2B_4O_7$ and 21.5% $LiBO_2$ at the University of Ottawa. Precision based on replicate run of 3 samples is ±0.35% for Al_2O_3, ±0.48% for MgO, ±1.3% for Cr, ±9.2% for Ni. The accuracy, which was monitored using international references of SY-2 and MRG-1, shows ±0.039% for Al_2O_3, ±0.28% for MgO, ±3.4% for Cr, ±4.0% for Ni. Precision and accuracy are less than 1 % and 10 % for other major and minor elements. Contents of PGE in bulk rocks were determined by isotopic dilution method using a mixed spike of ^{99}Ru, ^{105}Pd, ^{190}Os, ^{191}Ir, and ^{194}Pt after pre-concentration of PGE into a Ni–sulphide bead that was dissolved in 6 N HCl. The filtrate was dissolved in concentrated HNO_3 before analysis with Agilent HP 4500 inductively coupled plasma mass spectrometer (ICP-MS) at the University of Ottawa. Blanks were 0.0032 ng Ir/g flux, 0.0007 ng Os/g flux, 0.0026 ng Pt/g flux, 0.035 ng Pd/g flux, and 0.0049 ng Ru/g flux for this analysis. These values are negligible compared to amounts in the samples, and thus blank corrections were not applied to the results. The analytical quality was monitored by running two rock references: TDB-1 diabase from CANMET, Natural Resources of Canada; and JP–1 harzburgite from the Geological Survey of Japan. The values for the two are comparable to those obtained by Meisel and Moser (2004) (Table 1). The concentrations of S, Cu and Pb were determined using a Varian VISTA-PRO inductively coupled plasma-optical emission spectrometer (S, Cu) and Agilent HP 4500 ICP-MS (Pb) after digesting samples in *aqua regia* in screw-top Teflon vials for 48 hrs at 150 °C. The precision based on replicate runs of five samples is <11% for Cu, <7% for S and <12% for Pb.

5. Results

5.1. Mineral chemistry

5.1.1. Olivine

Olivine is replaced by pseudomorphic serpentine, and no primary silicate minerals are present in our serpentinite samples. In dunite, olivine compositions are similar among different grains in individual samples (Table 3, Fig. 4). Olivine contains consistently high MgO (Fo = 91.7–92.4), NiO (0.36–0.41 wt.%), and low CaO (≤0.02 wt.%). The contents of MnO are overall low ranging from 0.09 to 0.17 wt.%. The Fo vs. NiO values of olivine in our samples are distinctly higher than those of abyssal peridotites (Dick, 1989; Sobolev et al., 2005) (Fig. 4B), and the compositions of olivine and spinel grains from

Fig. 2. (A and B) Photomicrograph of serpentine (Serp) surrounded by talc (Tlc) and magnetite (Mag) in sample YKB3 and SLS2, under plane polarized light and crossed polarized light, respectively. (C) Photomicrograph of orthopyroxene (Opx) replaced by serpentine in sample YKB3, under crossed polarized light. (D) Photomicrograph of clinochlore (Clc) replacing orthopyroxene in sample YKB3. (E) Photomicrograph of primary olivine (Ol) surrounded by serpentine and fine-grained magnetite in sample HJL1, under plane polarized light. (F) Back-scattered electron image of a mixture of pentlandite (Pn) and pyrrhotite (Po) in the rim of an olivine grain in sample SLS2. The mixture is interpreted to be an exsolution product of once homogeneous monosulfide solid solution. (G) Back-scattered electron image of secondary magnetite and pentlandite surrounding chromite (Cr-spl) in serpentinite (sample YKB5). (H) Back-scattered electron image of chromite (light gray cores) rimmed by magnetite (white) in dunite (samples HJL2).

Please cite this article as: Xie, Z., et al., Origins of ultramafic rocks in the Sulu Ultrahigh-pressure Terrane, Eastern China, Lithos (2013), http://dx.doi.org/10.1016/j.lithos.2012.12.003

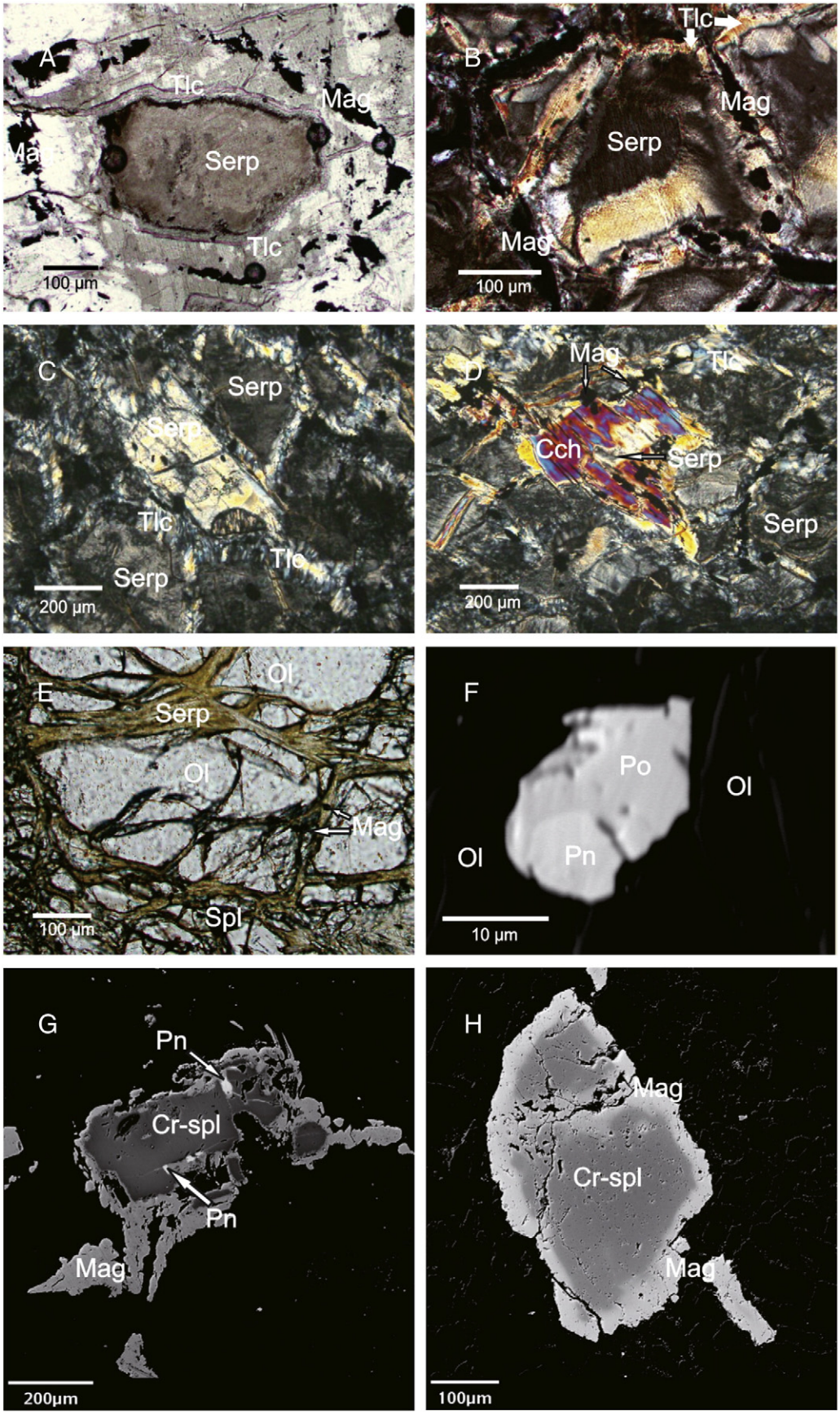

Please cite this article as: Xie, Z., et al., Origins of ultramafic rocks in the Sulu Ultrahigh-pressure Terrane, Eastern China, Lithos (2013), http://dx.doi.org/10.1016/j.lithos.2012.12.003

Table 3
Compositions of representative olivine grains from dunites.

Sample:	HJL1		HJL2		HJL3		HJL4	
Position:	Ol-c	Ol-r	Ol-c	Ol-r	Ol-c	Ol-c	Ol-c	Ol-r
SiO_2	41.27	41.54	41.04	40.96	41.11	42.25	41.13	41.20
Cr_2O_3	<0.01	<0.01	<0.01	0.02	<0.01	<0.01	<0.01	<0.01
FeO	7.62	7.72	8.07	7.91	7.61	7.54	7.59	7.72
MgO	50.19	50.87	50.12	50.18	50.62	51.33	50.10	50.54
MnO	0.12	0.13	0.13	0.17	0.12	0.12	0.13	0.12
NiO	0.40	0.40	0.41	0.39	0.38	0.39	0.38	0.39
CaO	0.01	0.01	0.02	0.01	0.01	0.01	0.01	<0.01
TOTAL	99.61	100.67	99.79	99.62	99.85	101.64	99.34	99.97
O = 4								
Si^{4+}	1.006	1.002	1.001	1.000	1.000	1.007	1.005	1.001
Cr^{3+}	0.000	0.000	0.000	0.000	0.000	0.000	0.000	0.000
Fe^{2+}	0.155	0.156	0.165	0.162	0.155	0.150	0.155	0.157
Mg^{2+}	1.823	1.829	1.822	1.827	1.835	1.825	1.825	1.831
Mn^{2+}	0.002	0.003	0.003	0.003	0.002	0.002	0.003	0.002
Ni^{2+}	0.008	0.008	0.008	0.008	0.007	0.008	0.008	0.008
Ca^{2+}	0.000	0.000	0.000	0.000	0.000	0.000	0.000	0.000
Sum	2.99	3.00	3.00	3.00	3.00	2.99	3.00	3.00
Fo	92.2	92.1	91.7	91.9	92.2	92.4	92.2	92.1

Note: Ol—Olinve; c—core, r—rim; Fo is the forsterite component, 100*(Mg/[Mg + Fe]).

dunite plot in the field of refractory peridotites in the olivine-spinel mantle array of Arai (1994) (Fig. 5).

5.1.2. Chromian spinel

Cr-spinel is common in serpentinite and dunite, and its rims are variably oxidized to magnetite (Fig. 2E, F). The boundaries between cores and oxidized rims are sharp and the cores of spinel grains show low Y_{Fe3+} ($Fe^{3+}/[Fe^{3+} + Al^{3+} + Cr^{3+}]$, 0.05–0.12) and TiO_2 (≤0.5 wt.%; Table 4). Furthermore, the core compositions of different grains are similar within individual samples (Table 4; Fig. 3), suggesting that the cores likely retain the primary compositions.

Cores of spinel grains in serpentinites show high Cr# (YKB 0.57–0.78; SLS 0.68–0.79) and low Y_{Fe3+} (YKB 0.08–0.12; SLS 0.06–0.09), and low X_{Mg} (atomic ratio of Mg/[Mg + Fe], YKB 0.22–0.33; SLS 0.29–0.38). In dunite, Cr–spinel has high Cr# (0.68–0.76) and low X_{Mg} (0.33–0.40), and the composition is very similar to the Cr-spinel from SLS serpentinites (Table 4; Fig. 3A). High Cr# suggests the refractory nature of the protoliths of serpentinite and dunite samples.

5.2. Bulk-rock compositions

5.2.1. Major elements

All serpentinites contain low contents of Al_2O_3 (YKB serpentinites: 1.57–2.10 wt.%; SLS serpentinites: 0.56–0.68 wt.%) and CaO (mostly ≤0.21 wt.%), and high MgO (YKB serpentinites: 37.5–39.2 wt.%; SLS serpentinites: 38.6–40.4 wt.%), Ni (≥1578 ppm) and Cr (≥2320 ppm) (Table 1). Bulk-rock Mg# values (= atomic ratio of Mg*100/[Mg + Fe_{total}] are high, ranging between 90.7 and 93.2. The contents of MgO in bulk serpentinites from SLS are slightly higher than those from YKB, and the contents of Al2O3, TiO_2 and V are lower for the former than the latter (Table 1; Fig. 6).

Dunites from HJL contain lower Al_2O_3 (≤0.40 wt.%) and CaO (≤0.85 wt.%), and higher bulk-rock Mg# (89.3–92.1) and Ni (≥1982 ppm) than the primitive mantle values (McDonough and Sun, 1995) (Table 1). It was noted that the bulk rock compositions of dunite are similar to those of SLS serpentinites (Table 1; Fig. 6).

5.2.2. Platinum group elements

Serpentinites contain high concentrations of Ir-type PGE (IPGE) (YKB serpentinites: Os = 3.9–4.7 ppb, Ir = 2.8–5.4 ppb, Ru = 6.1–6.7 ppb; SLS serpentinites: Os = 5.2–7.3 ppb, Ir = 3.0–8.4 ppb, Ru = 7.3–9.5 ppb) and ratios of IPGE to Pd–type PGE (PPGE) (YKB serpentinites: 1.2–1.8; SLS serpentinites: 4.9–5.5) (Table 1; Fig. 7A). Serpentinites from SLS contain slightly higher IPGE than the primitive mantle values and very low concentrations of PPGE, which makes high ratios of IPGE/PPGE (Table 1; Fig. 7A). High concentrations of IPGE and the high IPGE/PPGE ratios suggest that they are likely mantle residues after high degree of partial melting.

Table 4
Compositions of representative cr-spinel grains from serpentinites and dunites.

Lithology sample:	Serpentinite						Dunite			
	YKB3	YKB4	YKB5	SLS1	SLS2	SLS3	HJL1	HJL2	HJL3	HJL4
Cr-spinel										
SiO_2	<0.01	<0.01	<0.01	<0.01	0.08	0.01	0.03	<0.01	0.02	<0.01
TiO_2	0.34	0.30	0.24	0.19	0.29	0.19	0.39	0.29	0.32	0.25
Al_2O_3	13.56	13.35	14.10	11.86	12.49	10.96	10.96	11.76	14.73	14.97
Cr_2O_3	44.97	45.07	46.04	50.85	49.07	52.37	51.39	49.83	49.88	50.04
Fe_2O_3	9.05	8.89	8.37	6.02	7.38	5.25	6.40	7.38	4.42	4.75
FeO	24.28	25.97	25.51	24.11	23.85	23.99	22.96	23.01	22.61	21.92
MgO	5.98	4.88	5.56	6.04	6.43	5.95	6.83	6.84	7.55	8.08
MnO	0.45	0.49	0.37	0.49	0.46	0.54	0.40	0.37	0.40	0.39
NiO	0.07	0.10	0.11	0.06	0.07	0.04	0.08	0.10	0.06	0.07
Sum	98.70	99.05	100.30	99.62	100.04	99.29	99.41	99.58	99.97	100.47
O = 32										
Si^{4+}	0.000	0.000	0.000	0.000	0.020	0.003	0.008	0.000	0.005	0.000
Ti^{4+}	0.069	0.062	0.048	0.039	0.058	0.040	0.079	0.058	0.065	0.050
Al^{3+}	4.346	4.303	4.455	3.791	3.959	3.530	3.506	3.744	4.581	4.616
Cr^{3+}	9.668	9.744	9.760	10.905	10.430	11.312	11.028	10.641	10.410	10.350
Fe^{+3}	1.852	1.829	1.688	1.229	1.492	1.080	1.306	1.500	0.878	0.936
Fe^{2+}	5.520	5.938	5.720	5.468	5.364	5.481	5.211	5.197	4.991	4.796
Mg^{2+}	2.425	1.990	2.222	2.443	2.578	2.423	2.761	2.753	2.971	3.151
Mn^{2+}	0.104	0.113	0.085	0.112	0.105	0.124	0.091	0.085	0.090	0.086
Ni^{2+}	0.015	0.022	0.023	0.012	0.014	0.009	0.017	0.022	0.013	0.015
Sum	24.00	24.00	24.00	24.00	24.00	24.00	24.00	24.00	24.00	24.00
$Cr^{\#}$	0.69	0.69	0.69	0.74	0.72	0.76	0.76	0.74	0.69	0.69
YFe^{3+}	0.12	0.11	0.10	0.08	0.09	0.07	0.08	0.09	0.05	0.06
X_{Mg}	0.31	0.25	0.28	0.31	0.32	0.31	0.35	0.35	0.37	0.40

Note: FeO and Fe_2O_3 contents of Cr-spinel were calculated assuming a stoichiometric compositions; $Cr^{\#}$ = atomic ratio of Cr/(Cr + Al) in Cr-spinel, YFe^{3+} = atomic ratio of $Fe^{3+}/[Fe^{3+} + Al + Cr^{3+}]$, X_{Mg} = atomic ratio of $Mg/(Mg + Fe^{2+})$.

Please cite this article as: Xie, Z., et al., Origins of ultramafic rocks in the Sulu Ultrahigh-pressure Terrane, Eastern China, Lithos (2013), http://dx.doi.org/10.1016/j.lithos.2012.12.003

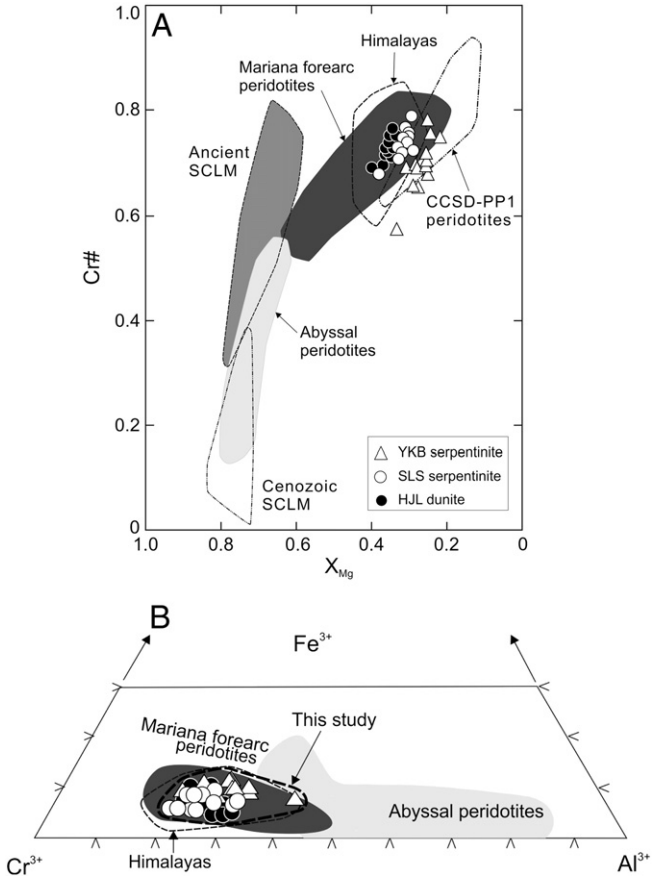

Fig. 3. The composition of spinel cores from serpentinites and dunites in the Sulu belt. Each point represents the composition of one grain in our ultramafic rocks. The data sources: abyssal peridotite is from Dick and Bullen (1984) and Barnes and Roeder (2001), the Mariana forearc field (Ishii et al., 1992), the Himalayan forearc mantle peridotites (Hattori and Guillot, 2007), forearc mantle peridotites in Dominican Republic (Saumur et al., 2010). Ancient subcontinental lithospheric mantle (SCLM) values were represented by mantle xenoliths in Paleozoic kimberlites (Mengyin area), Mesozoic diorite (Fushan area), Mesozoic basalt (Junan area), and Cenozoic basalt (Hebi area) in the eastern NCC, obtained by Zheng et al. (2001, 2006), Ying et al. (2006), and Xu et al. (2010). Cenozoic SCLM are xenoliths in Late Cretaceous basalt (Junan area) and Cenozoic basalt (Hebi, Shangwang, Junan and Changbaishan areas) obtained by Zheng et al. (2006), Ying et al. (2006), and Wang et al. (2012b). The field for CCSD-PP1 peridotites is after Zheng et al. (2006). (A) Plot of Cr# vs. X_{Mg} of Cr-spinels. Note the similar trends for YKB, SLS serpentinites and HJL dunites compared to those from the forearc peridotites field and the CCSD–PP1 peridotites field. (B) Ternary (Fe^{3+}–Cr^{3+}–Al^{3+}) diagram for Cr-spinel in our ultramafic rocks. Note that the compositions of spinel in our ultramafic rocks are similar to those of forearc mantle peridotite from the Himalayas and Marianas.

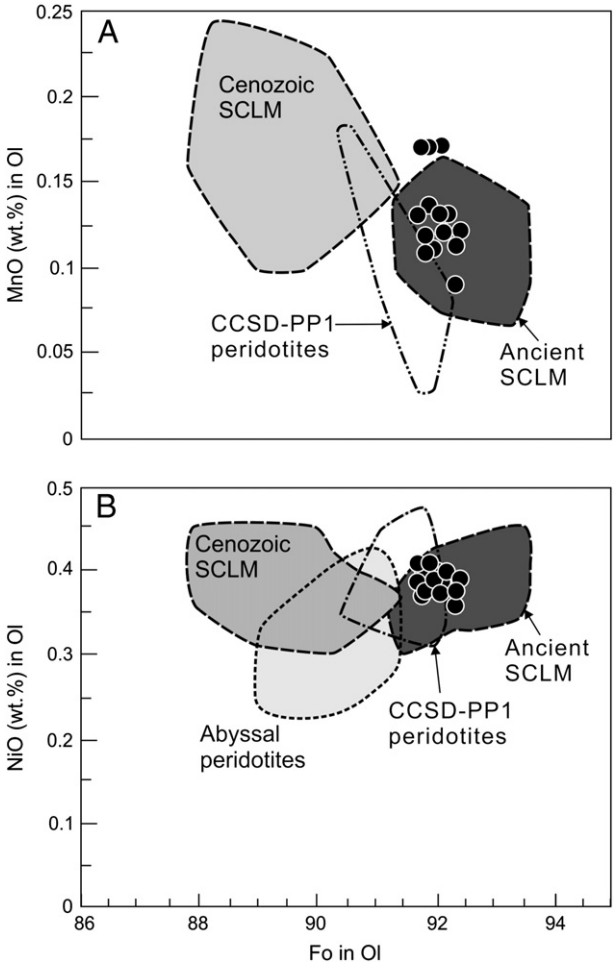

Fig. 4. Contents of MnO and NiO vs. Fo values of olivine (Ol) from HJL dunite samples. The gray field for most abyssal peridotites is after Dick (1989) and Sobolev et al. (2005). Other symbole are same as in Fig. 3. Note that the compositions of olivine in our samples are similar, and our dunites probably represent ancient lithospheric mantle underlying the SE margin of the NCC.

Dunite samples from HJL contain high concentrations of IPGE (Os = 1.1–7.8 ppb, Ir = 1.7–3.6 ppb, Ru = 2.1–11.2 ppb) and ratios of IPGE/PPGE (up to 8.8) (Table 1; Fig. 7B). The primitive mantle-normalized PGE pattern and high ratios of IPGE/PPGE suggest that they are also residual mantle peridotites after extensive partial melting. In addition, the PGE abundances and patterns of HJL dunites are similar to those of SLS serpentinites.

5.2.3. Copper, sulphur and lead

Serpentinites and dunites contain very low contents of Cu (≤3.7 ppm except 40.1 ppm for YKB4), and various concentrations of S (52–171 ppm for YKB serpentinites, 240–310 ppm for SLS serpentinites, 20–65 ppm for HJL dunites) and Pb (average 8.3 ppm for YKB serpentinites, 5.3 ppm for SLS serpentinites, 0.9 ppm for HJL dunites; Table 1). Copper, S, and Pb are incompatible in mantle silicate minerals and are removed from the mantle during partial melting, but our samples show varying concentrations of these elements with no correlations between Cu and S and between Ni and S (Fig. 9A and B). The data suggest that S and also Cu may have been introduced later. The interpretation is supported by the occurrence of sulphides in close spatial association with serpentine. Sulphur was likely introduced during the serpentinization.

Sulphide would concentrate PGEs as the partition coefficients between sulphide and silicate melt are very high, >1,000 (e.g., Crocket et al., 1997), but the S contents are not correlated with the contents of PGEs (Fig. 9C). The data are consistent with the petrographic evidence for late introduction of S.

The Pb concentrations in our serpentinite samples range from 0.3 to 10.1 ppm (Table 1). The values are high compared to the primitive mantle value of 0.15 ppm (McDonough and Sun, 1995), suggesting the late introduction of Pb.

6. Discussion

6.1. Protoliths and origins of ultramafic rocks

6.1.1. Serpentinite

The tectonic setting of the protoliths of serpentinites in orogenic belts have been discussed extensively (e.g., Hattori and Guillot, 2007; Saumur et al., 2010). There are three possible origins for serpentinites: 1) forearc mantle peridotites; 2) abyssal peridotites; 3) cumulates of mafic melt either in the overlying plate or in the incoming plate.

The compositions of spinel plot within or close to the field of Marianan forearc mantle peridotites (Cr# up to 0.82; Ishii et al.,

Please cite this article as: Xie, Z., et al., Origins of ultramafic rocks in the Sulu Ultrahigh-pressure Terrane, Eastern China, Lithos (2013), http://dx.doi.org/10.1016/j.lithos.2012.12.003

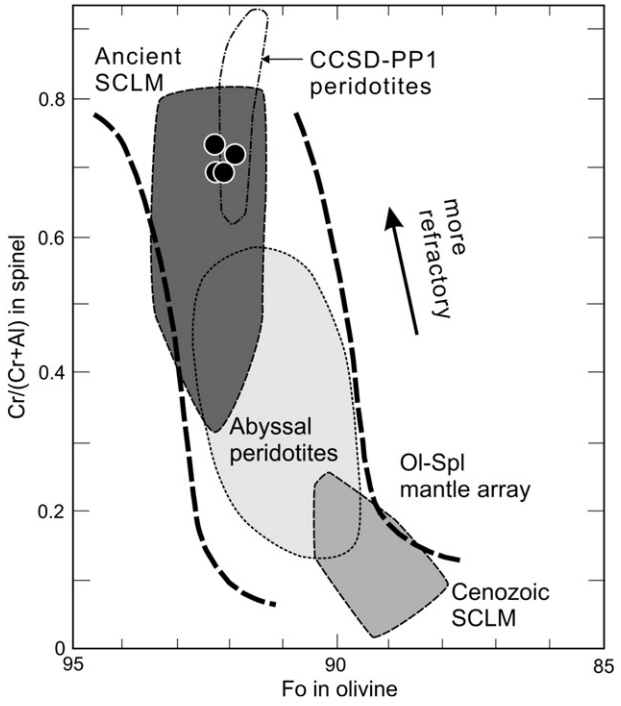

Fig. 5. Forsterite component of olivine versus Cr# of Cr–spinel. The compositional range of mantle peridotites (Ol–Spl mantle array) and abyssal peridotites (gray field) are from Arai (1994). Other symbols are same as in Fig. 3. Note that dunite samples from HJL all plot in the mantle array, and they probably represent the ancient lithospheric mantle.

1992) and Himalayan forearc serpentinites (Cr# up to 0.84; Hattori and Guillot, 2007), and show distinctly higher Cr# and lower X_{Mg} than those observed in abyssal peridotites in Cr# vs. X_{Mg} diagram (Fig. 3A). Cr# of spinel in the residual peridotite increases after partial melting because Al is preferentially incorporated into a melt. Therefore, the values of Cr# for spinel are high in mantle wedges and relatively low in abyssal peridotites. The values for abyssal peridotites rarely exceed 0.60 (Dick and Bullen, 1984). The data from our samples, Cr# up to 0.79, suggest that the protoliths are most likely residual mantle peridotites after extensive partial melting in the mantle wedge, but high Cr# of spinel is also found cumulates of primitive melt formed from such refractory mantle peridotites. We

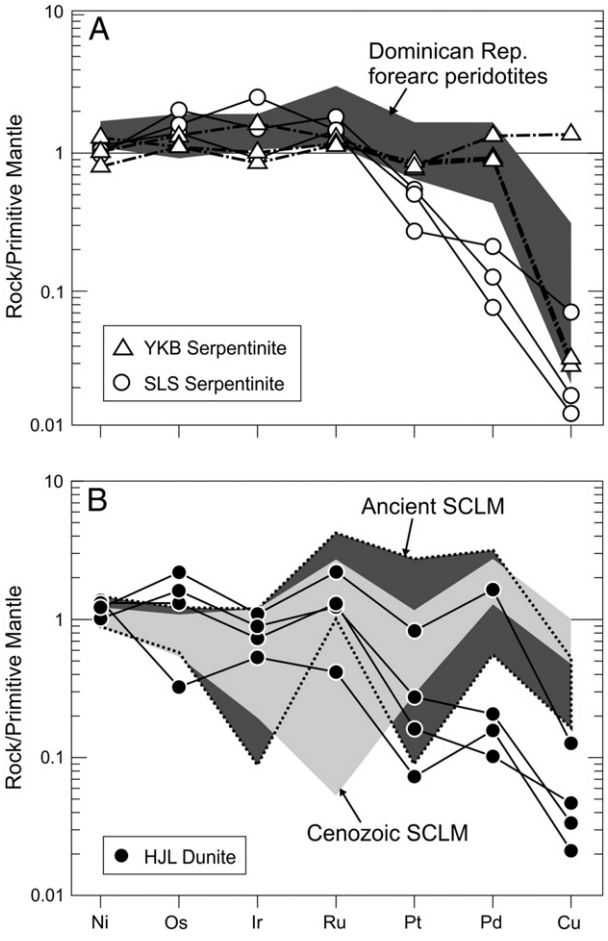

Fig. 7. Primitive mantle-normalized values of PGE, Ni, and Cu in serpentinites and dunites from the Sulu belt. Elements are placed in order of decreasing compatibility. PGE values for the primitive mantle are 0.00725 times of those of carbonaceous chondrites (CI) (McDonough and Sun, 1995). The field for Dominican Republic is after Saumur et al. (2010), and the ancient and Cenozoic SCLM in the eastern NCC (E. NCC) are after Zheng et al. (2005b). In general, the high content in Ir-group PGEs and high ratios of IPGE/PPGE suggest that serpentinites and dunite were residual mantle peridotites, not ultramafic cumulates. (A) Data from YKB and SLS serpentinite samples. (B) Data from HJL dunite samples.

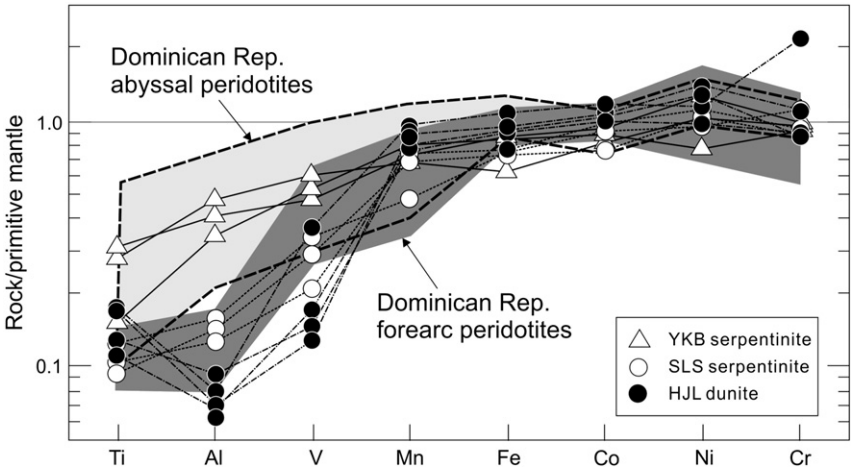

Fig. 6. Primitive mantle-normalized immobile elements from Sulu serpentinites and dunites. Positive slopes suggest depletion of incompatible elements compared to compatible elements, and our samples are the mantle residues. Moreover, samples from the SLS and HJL are more depleted in Ti, Al, and V compared to samples from YKB. The data from the Dominican Republic forearc serpentinites are from Saumur et al. (2010). Primitive mantle values are from McDonough and Sun (1995).

Please cite this article as: Xie, Z., et al., Origins of ultramafic rocks in the Sulu Ultrahigh-pressure Terrane, Eastern China, Lithos (2013), http://dx.doi.org/10.1016/j.lithos.2012.12.003

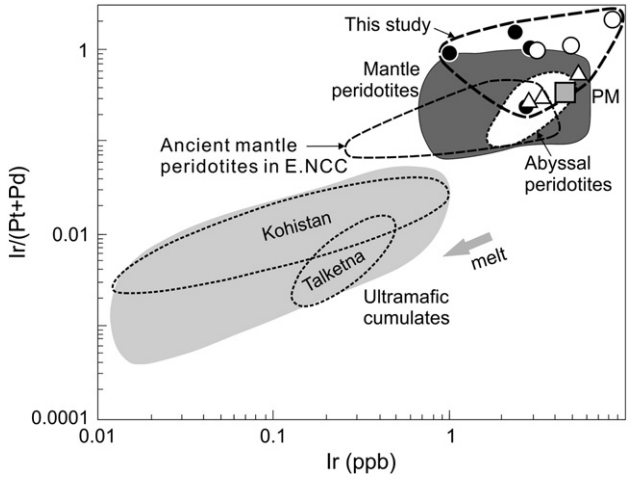

Fig. 8. Ratios of Ir/(Pt + Pd) versus the contents of Ir (ppb) for our ultramafic rocks. Primitive mantle value is shown with gray squares, labeled PM (McDonough and Sun, 1995). The field for mantle peridotites includes abyssal peridotites (Rehkämper et al., 1999); Horoman, Japan (Rehkämper et al., 1999); Zabargad, Red Sea, and Ronda, Spain, plus forearc mantle serpentinites in Himalayas (Hattori and Guillot, 2007). The field for ultramafic cumulates includes data from the Jijal ultramafic complex of the Kohistan Arc, Pakistan, and Talkeetna Arc, Alaska (Hattori and Guillot, 2007). The field of ancient mantle xenoliths in the eastern NCC (E. NCC) is defined by mantle xenoliths at Xinyang and Hebi areas in the eastern NCC mantle (Zheng et al., 2005b). The symbols are the same in Fig. 6. Note that serpentinites (YKB and SLS) and dunite (HJL) contains high Ir and plot in the field of mantle peridotites. The field of the ancient mantle xenoliths in the eastern NCC (E. NCC) is after Zheng et al. (2005b). The symbols are the same in Fig. 6. Note that serpentinites (YKB and SLS) and dunite (HJL) contains high Ir and plot in the field of mantle peridotites.

discount the latter possibility because our Cr-spinel shows similar compositions in individual study areas. Cr-spinel in cumulates commonly shows a large variation in Cr# as Cr is quickly removed from a melt during its solidification. Our proposed interpretation is further supported by PGE data. Cumulates show low ratios of IPGE to PPGE because of the preferential retention of IPGE in the residues during the partial melting (Hattori and Hart, 1997; Wang et al., 2012a). Our samples show consistently high concentrations of IPGE and high ratios of IPGE to PPGE. Therefore, we conclude that the protoliths of our serpentinites are residual mantle peridotites after high degrees of partial melting in the mantle wedge below the margin of the NCC. They are not ultramafic cumulates (Figs. 7A and 8).

The contents of Fe^{3+} in spinel in our serpentinites are similar to those of Himalayan serpentinites (Y_{Fe3+}, 0.04–0.13; Hattori and Guillot, 2007), and slightly higher than the values of forearc serpentinites from the Marianas (Y_{Fe3+}, ≤0.08; Ishii et al., 1992). High Y_{Fe3+} values usually reflect high fO_2 (Canil et al., 1994; Wang et al., 2008a), suggesting that the protoliths of serpentinites from YKB and SLS had high fO_2. Slightly oxidized conditions are common in mantle wedges due to an influx of slab-derived melts and fluids (e.g., Parkinson and Arculus, 1999; Wang et al., 2012a).

The proposed interpretation, the mantle wedge origin of serpentinites, is further supported by relatively high contents of Pb (Table 1). Lead is commonly enriched in mantle wedge serpentinites as it is released from subducted slabs (e.g., Hattori and Guillot, 2003, 2007; Saumur et al., 2010). There is a possibility that Pb may have been introduced from the surrounding granitic gneiss during the exhumation as Pb is also high in continental crustal rocks. We discount this possibility because Pb concentrations are not correlated with the concentrations of other soluble elements, such as alkalis. Granitic gneisses contain high contents of alkalis (e.g., Tang et al., 2008). If peridotites were hydrated during the exhumation with gneisses, serpentinites would be enriched in alkalis and other fluid-mobile elements from the surrounding granitic gneisses. Serpentinite samples contain low concentrations of alkalis, lower than 0.005 wt.% for Na_2O and 0.01 wt.% or lower for K_2O (Table 1). The data suggest very little input of elements from the surrounding granitic gneisses. It is, therefore, reasonable to propose that Pb was introduced to serpentinites in the mantle wedge before the exhumation, as documented in serpentinites from several subduction zones by Hattori and Guillot (2003, 2007). Furthermore, low Al contents suggest little mechanical mixing with the surrounding granitic gneisses during the exhumation. Therefore, high concentrations of Pb in samples and relatively high Y_{Fe3+} values in Cr-spinel suggest that the protoliths of our serpentinites were in the mantle wedge, probably near the base of the mantle wedge close to the subducted slab.

The protolith of YKB serpentinites is harzburgite based on the abundance of orthopyroxene pseudomorphs (≥15 vol.%) in samples (Table 2; Fig. 2C). On the other hand, the protolith for the SLS serpentinite was probably dunite based on abundant olivine pseudomorphs in the samples. The interpretation is supported by the concentrations of moderately incompatible elements (Al, Ti, and V) in bulk rocks. Harzburgites contain higher concentrations of these elements than dunite (e.g., Wang et al., 2008a; Xu et al., 2008). The concentrations of these elements are higher in YKB serpentinites than SLS serpentinites (Table 1; Fig. 6).

Refractory dunites and harzburgites with high Cr# are common in mantle wedges, but not in the oceanic lithosphere. Therefore, we suggest that both SLS serpentinites and HJL dunites likely originated from the mantle wedge below the margin of NCC. The two show very similar Cr# values at given X_{Mg} in Cr-spinel and bulk–rock compositions (Figs. 3A, 6). The data suggest that SLS serpentinites were similar to HJL dunite before their hydration. One is totally hydrated and the other is partially hydrated, which reflects the dissimilar degrees of hydration in the mantle wedge. Heterogeneous hydration and distribution of serpentinites are common in the mantle wedge as demonstrated by different degrees of hydration in Mariana forearc peridotites and serpentinites (e.g., Ishii et al., 1992).

6.1.2. Dunite

There are several possible origins for dunites: 1) cumulate of mafic melt (e.g., Kelemen et al., 1995); 2) product of melt-peridotite reaction (e.g., Kelemen, 1990); 3) mantle residue after extensive partial melting (e.g., Hattori et al., 2010b). Dunite is common as xenoliths in late Mesozoic igneous rocks in the eastern NCC. The origin of these xenoliths is also debated. Proposed hypotheses include a residue after high degree of partial melting in the mantle (e.g., Xu et al., 2008; Zheng et al., 2001), cumulates of mafic melt (Wang et al., 2012a), and a reaction product of melt–peridotite (e.g., Xu et al., 2010).

The consistently high Fo of olivine, from 91.7 to 92.4, together with high Cr# in Cr-spinel of dunite samples plot in the refractory peridotite field in the olivine–spinel mantle array of Arai (1994) (Fig. 5). The evidence suggests that HJL dunites are residual mantle peridotites in the mantle wedge below the NNC. The interpretation is consistent with their high contents of compatible elements (Cr, Ni, and Mg) and low contents of mildly incompatible elements (Al, Ti, and V) in bulk rock compositions (Table 1; Fig. 6). The residual mantle origin of our dunite samples is further supported by high ratios of IPGE to PPGE (Table 1; Fig. 7B). Partial melting fractionates PGE, resulting in higher ratios of IPGE/PPGE in the residues and lower ratios in the melt (e.g., Brenan et al., 2005; Righter et al., 2004).

Olivine in our samples contain very low contents of CaO (≤0.02 wt.%). The data suggest a lithospheric mantle origin of the dunite samples. The CaO content is a function of temperature and olivine formed at low temperatures contains low CaO and that of magmatic origin contains high CaO, >0.10 wt.% (e.g., De Hoog et al., 2010).

We reject the cumulate origin for our dunite samples because cumulate formed from mafic melt, even in the upper mantle, contains low

Please cite this article as: Xie, Z., et al., Origins of ultramafic rocks in the Sulu Ultrahigh-pressure Terrane, Eastern China, Lithos (2013), http://dx.doi.org/10.1016/j.lithos.2012.12.003

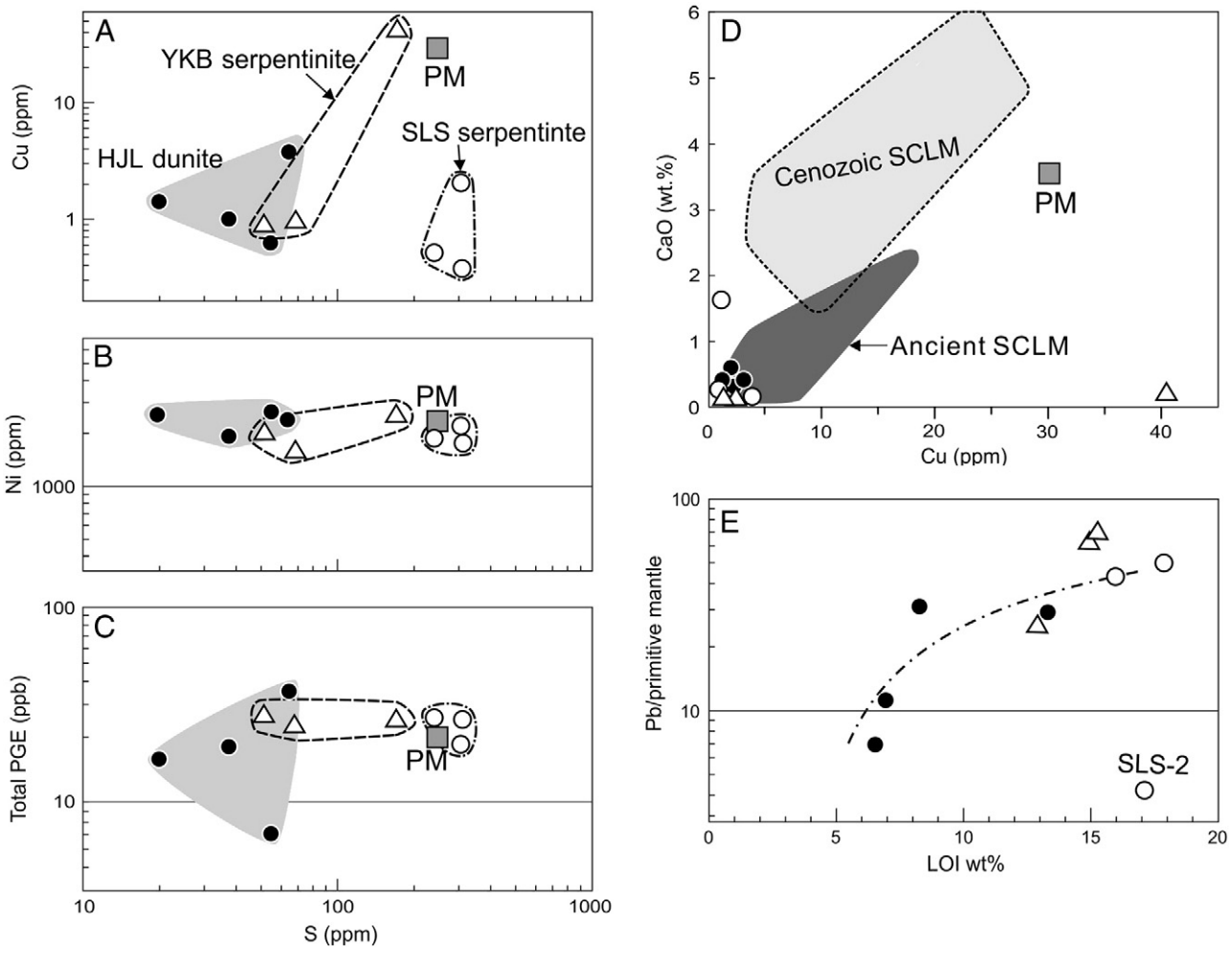

Fig. 9. Bulk chemical compositions of serpentinites and dunites from Sulu belt, eastern China. (A), Cu vs. S; (D), Ni vs. S; and (E), total platinum group elements (PGE) vs. S. (D), CaO vs. Cu; (E), loss on ignition (LOI) values vs. primitive mantle-normalized Pb contents in bulk-rocks. Data source for peridotites: Primitive mantle (PM) values are from McDonough and Sun (1995); Ancient SCLM in the eastern NCC (E. NCC) represented by mantle xenoliths at Xingyang, Hebi, and Fushan (Xu et al., 2010; Zheng et al., 2005b), and Cenozoic SCLM in the eastern NCC represented by mantle xenoliths at Shangwang and Changbaishan (Wang et al., 2012b; Zheng et al., 2005b). Filled symbols are the same as in Fig. 7. Note that our ultramafic rocks are highly refractory in terms of major elements, but serpentinites are relatively enriched in S compared to dunites. Moreover, S contents are not correlated with the PGEs, suggesting that sulphides are not the major host of PGE in our samples. In addition, the correlation between LOI and primitive mantle-normalized Pb contents confirmed that Pb was introduced with water during the hydration.

ratios of IPGE to PPGE (e.g., Wang et al., 2008b, 2012a). In addition, cumulate origin is not supported by consistently low TiO_2 (≤0.5 wt.%) in Cr-spinel in our dunites (Table 4), because cumulate dunite commonly contain high Ti and variable Cr in chromite (e.g., Melcher et al., 1997).

Dunite may form from harzburgite as a metasomatic product by reacting with mafic melt as proposed by Kelemen (1990), but this possibility is not applicable to our samples because of consistently high Mg and Ni within and between olivine grains (Table 3; Fig. 4). Olivine in metasomatized rocks commonly shows variable Mg content after reacting with a mafic/silicate melt (e.g., Wang et al., 2008b; Xu et al., 2010). Furthermore, dunite bodies formed by metasomatism commonly contain remnants of pre-metasomatic rocks and reaction zones between them (e.g., Quick, 1981). There is no evidence supporting the existence of pre-metasomatic harzburgitic rock in our dunite bodies.

Therefore, we conclude that HJL dunites originated from residual mantle peridotites and formed as the result of high degrees of partial melting after influx melting of clinopyroxene followed by exhaustion of orthopyroxene in the mantle wedge. The occurrence of such highly refractory dunite has been suggested in the eastern NCC by Xu et al. (2008) and in the eastern margin of Asian continent by Hattori et al. (2010b). The residual mantle dunite is not well documented, but it may be more abundant below Archean SCLM than commonly recognized (e.g., Griffin et al., 2009).

6.2. Comparison with ultramafic rocks underlying the North China Craton

6.2.1. Comparison of studied samples with mantle peridotite xenoliths in the North China Craton

The NCC is the largest and oldest cratonic block in China and its crust was formed in Archean time (e.g., Wu et al., 2005). The NCC has shown a stable craton since it is completely cratonization (~1.8–1.9 Ga) (Zhao et al., 2001), and it underwent a significant modification of the craton and lithospheric thinning process during the Phanerozoic period (Xu, 2001; Zhu et al., 2012). A thick (≥200 km), cold and refractory lithosphere was removed and replaced by asthenospheric material, which is hot and fertile, and the thickness of the SCLM in the eastern China is less than 80 km at present (e.g., Kusky et al., 2007).

The change in the SCLM of the NCC is evaluated from peridotite xenoliths brought to the surface by explosive igneous rocks of various age. They include xenoliths in Paleozoic kimberlites (e.g., Mengyin, Fuxian), Mesozoic diorites and basalts (e.g., Fushan, Junan), and Cenozoic basalts (e.g., Hebi, Shangwang, Changbaishan). These mantle peridotites were

Please cite this article as: Xie, Z., et al., Origins of ultramafic rocks in the Sulu Ultrahigh-pressure Terrane, Eastern China, Lithos (2013), http://dx.doi.org/10.1016/j.lithos.2012.12.003

well studied in the last decade (Wang et al., 2012b; Wu et al., 2005; Xu, 2001; Xu et al., 2008, 2010; Zheng et al., 2006, 2007), and were classified into two distinctive groups based on mineral assemblages and bulk rock compositions: the relict Archean SCLM and newly formed Cenozoic SCLM. The peridotites of the relict Archean SCLM are harzburgites, lherzolites, and minor dunites (e.g., Zheng and Lu, 1999; Zheng et al., 2001). They are refractory with high Fo (> 92) in olivine, low abundance of clinopyroxene, and low concentrations of incompatible elements (Al, Ti, and V). In contrast, the new Cenozoic SCLM is mostly lherzolite and fertile with low Fo (<90) and abundant clinopyroxene (e.g., Wang et al., 2012b; Zheng et al., 2005b).

Mineral chemistry and bulk rock compositions of our samples are relatively different from those of Cenozoic SCLM that have been brought to the surface as peridotite xenoliths in Hebi, Shangwang, Junan, Changbaishan areas reported by Zheng et al. (2006), Ying et al. (2006), and Wang et al. (2012b). Instead, the geochemical features of our samples are similar to those of the refractory ancient SCLM reported from peridotite xenoliths in Hebi, Mengyin, Junan, and Fushan by Zheng et al. (2001, 2006), Ying et al. (2006), and Xu et al. (2010) (Figs. 3A, 4, 5). The abundance of PGE is also similar to those from Hebi and Xinyang reported by Zheng et al. (2005b). The data confirm that the ultramafic rocks in this study probably represent the ancient SCLM underlying the southeastern margin of the NCC.

The Cr contents of spinel in our samples are even slightly higher than those of the ancient SCLM peridotites (Fig. 3A). In addition, our rocks (except sample SLS2 and YKB4) show very low concentrations of incompatible elements, such as Cu and CaO, compared to the ancient SCLM in the eastern NCC reported by Zheng et al. (2005b) and Xu et al. (2010) (Fig. 9D). The data suggest that the peridotites from the Sulu belt are more refractory than the ancient SCLM peridotites underlying the NCC. Alternatively, the increase in Cr contents and decrease in Cu and CaO contents in our samples are attributed to the HP to UHP metamorphism of peridotites in the Sulu belt. We discount this possibility because it requires a decrease in modal abundance of spinel, a loss of Al or a gain of Cr in the rocks during HP–UHP metamorphism. Bulk rock Cr/Al ratios and the modal abundance of spinel are similar between our samples and the SCLM peridotites. Furthermore, the protoliths of our samples are dunite and harzburgite, whereas the ancient SCLM mainly consists of harzburgites and lherzolites. The protoliths of our samples have more refractory lithologies than the ancient SCLM. Therefore, our data suggest that high Cr# in spinel is not related to the metamorphism, and that the studied ultramafic rocks likely have been subjected to higher degree of partial melting than the ancient SCLM.

The southeastern NCC was an active margin forming a continental arc during the closure of the Tethyan sea before the collision with the YZC (e.g., Zhao et al., 2001). We suggest that the mantle wedge below the margin of the NCC became highly refractory during the subduction of the Tethyan oceanic lithosphere through the partial melting.

6.2.2. Comparison of studied samples with other ultramafic rocks in the Dabie–Sulu belt

In the Dabie–Sulu UHP terrane, most peridotite bodies (e.g., Yangkou and Donghai areas in the Sulu belt and Raobazhai area in the Dabie belt) were recognized as fragments of the ancient SCLM (Tsai et al., 2000; Ye et al., 2009; Zhang et al., 2005, 2008; Zheng et al., 2005a, 2006). The garnet-bearing peridotites, recovered during the drilling of the pre-pilot hole of the Chinese Continental Scientific Drilling Project (CCSD–PP1) at Zhimafang, ~120 km from SLS and HJL study areas (Fig. 1A), are considered to represent refractory ancient SCLM (e.g., Zhang et al., 2008; Zheng et al., 2005a, 2006). In the Dabie belt, Raobazhai ultramafic bodies are interpreted as a fragment of the ancient SCLM of the NCC, and their protolith was derived from the spinel field of the mantle wedge below the NCC (Zheng et al., 2008).

Our ultramafic rocks show similar compositions of olivine and spinel to garnet-bearing peridotites recovered by the drilling of CCSD-PP1 (Figs. 3A, 4, 5), suggesting that similar refractory nature between our samples and the protoliths of the CCSD-PP1 peridotites. These CCSD-PP1 peridotites were subjected to UHP metamorphism (e.g., Ye et al., 2009; Zhang et al., 2005). Our samples contain spinel grains with no evidence of relict garnet or the transformation of spinel to garnet. Furthermore, the ultramafic bodies in the HJL and SLS areas contain spinel-bearing peridotites (e.g., Gao et al., 2004; Yang, 2006; Zhang and Liou, 2003). Therefore, we consider that these ultramafic rocks have not undergone UHP metamorphism. If our ultramafic rocks were metamorphosed under high pressures, ~5 GPa (Ye et al., 2000) as the eclogite and garnet peridotites, serpentine is unstable and should be dehydrated to form the secondary olivine. There is no evidence suggesting that olivine in our samples recrystallized from serpentine. Recrystallized olivine commonly contains magnetite inclusions, but olivine grains in our samples are essentially inclusion-free.

The area was an active continental margin during the closure of the Tethyan Sea by the subduction of the oceanic lithosphere, and underwent subsequent collision and subduction of the margin of the YZC. The nature of the subduction evolved with time from the oceanic subduction to continental subduction, and the interface, subduction channel, between the NCC and subducted lithosphere also experienced substantial changes. Oceanic lithosphere was subducted to a deep level forming dense eclogites and some were exhumed to the surface by a return flow in the subduction channel (e.g., Guillot et al., 2009). Mantle wedge peridotites may be dragged down to the subduction channel by mantle flow for a later exhumation (e.g., Hattori et al., 2010a,b). In the Sulu belt, this oceanic subduction was followed by the collision and subduction of the continental rocks of the YZC. Granitic continental

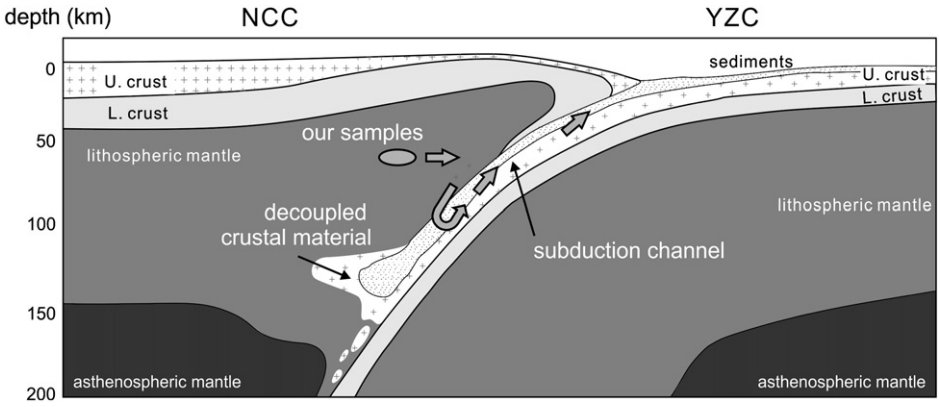

Fig. 10. Schematic diagram showing the incorporation of studied peridotites into the subduction channel and exhumation in the subduction channel in the Sulu belt, based on the numerical models by Warren et al. (2008) and Li and Gerya (2009). U. crust = upper crust; L. crust = lower crust.

Please cite this article as: Xie, Z., et al., Origins of ultramafic rocks in the Sulu Ultrahigh-pressure Terrane, Eastern China, Lithos (2013), http://dx.doi.org/10.1016/j.lithos.2012.12.003

rocks have low density compared to the surrounding mantle rocks. Many numerical models suggest that this buoyancy of granitic rocks results in the decoupling of blocks from the rest of subducted lithosphere (e.g., Li and Gerya, 2009; Warren et al., 2008) (Fig. 10). Once this decoupling develops, peridotites incorporated from the mantle wedge would not be subducted to a deep level and they may be easily exhumed together with the upward movement of granitic rocks. This may be the reason why the mantle wedge peridotites incorporated into the subduction channel had a short loop shallow subduction and exhumation with the granitic material. We suggest that our samples represent such mantle wedge peridotites dragged down to the subduction channel by a mantle flow, subducted to a relatively shallow level and exhumed together with granitic gneiss in the return flow of the subduction channel (Fig. 10).

7. Conclusions

Bulk rock and mineral compositions suggest the ultramafic rocks in the Sulu UHP belt originated from the forearc mantle peridotites overlying the subducted YZC and underlying the eastern margin of the NCC. The protoliths of serpentinites from YKB and SLS are most likely harzburgite and dunite, respectively. SLS serpentinites have similar bulk rock and mineral compositions as HJL dunites, suggesting that both may have originated from similar portions in the mantle wedges. Both are refractory residual mantle peridotites after extensive partial melting compared to the protolith of YKB serpentinites.

The ultramafic rocks likely represent fragments of ancient SCLM beneath the southeastern NCC, and became more refractory during the subduction of the Tethyan oceanic lithosphere before the collision with the YZC. Compared to garnet–bearing peridotites in the Sulu belt, our ultramafic rocks were likely derived from shallow parts (e.g. spinel-stable field) of mantle wedge beneath the eastern NCC, incorporated into the subduction channel, and exhumed together with the granitic rocks of Yangtze continental crust in the subduction channel.

Acknowledgements

This research was carried out as part of the senior author's Ph.D. thesis research. The senior author thanks the University of Ottawa for accepting him as a visiting student in the summer of 2011 to conduct the analytical aspect of this research. We also thank Nimal De Silva, Smita Mohanty, and Peter Jones for their help during the chemical analysis of samples at the University of Ottawa and Carlton University. The project was financially supported by a grant from the Natural Science and Engineering Research Council of Canada to KH, grants from the National Natural Science Foundation of China (numbers: 41173034, 90814003) and China Geological Survey (number: 1212011121088), and a grant from Graduate Innovation Fund of Jilin University (number: 20121072).

References

Arai, S., 1994. Characterization of spinel peridotites by olivine-spinel compositional relationships: review and interpretation. Chemical Geology 111, 91–204.
Barnes, S.J., Roeder, P.L., 2001. The range of spinel compositions in terrestrial mafic and ultramafic rocks. Journal of Petrology 42, 2279–2302.
Brenan, J.M., McDonough, W.F., Ash, R., 2005. An experimental study of the solubility and partitioning of iridium, osmium and gold between olivine and silicate melt. Earth and Planetary Science Letters 237, 855–872.
Canil, D., O'Neill, H., St, C., Pearson, D.G., Rudnick, R.L., McDonough, W.F., Carswell, D.A., 1994. Ferric iron in peridotites and mantle oxidation states. Earth and Planetary Science Letters 123, 205–220.
Crocket, J.H., Fleet, M.E., Stone, W.E., 1997. Implications of composition for experimental partitioning of platinum-group elements and gold between sulfide liquid and basalt melt: the significance of nickel content. Geochimica et Cosmochimica Acta 61, 4139–4149.
De Hoog, J.C.M., Gall, L., Cornell, D.H., 2010. Trace-element geochemistry of mantle olivine and application to mantle petrogenesis and geothermobarometry. Chemical Geology 270, 196–215.
Dick, H.J.B., 1989. Abyssal peridotites, very slow spreading ridges and ocean ridge magmatism. In: Saunders, A.D., Norry, M.J. (Eds.), Magmatism in the ocean basins: Geological Society, London, Special Publication, 42, pp. 71–105.
Dick, H.J.B., Bullen, T., 1984. Chromian spinel as a petrogenetic indicator in abyssal and alpine-type peridotites and spatially associated lavas. Contributions to Mineralogy and Petrology 86, 54–76.
Gao, T.S., Chen, J.F., Xie, Z., Yang, S.H., Yu, G., 2004. Zircon SHRIMP U–Pb age of garnet olivine pyroxenite at Hujialin in the Sulu terrane and its geological significance. Chinese Science Bulletin 49 (20), 2198–2204.
Griffin, W.L., O'Reilly, S.Y., Afonso, J.C., Begg, G.C., 2009. The composition and evolution of lithospheric mantle: a re-evaluation and its tectonic implications. Journal of Petrology 50, 1185–1204.
Guillot, S., Hattori, K.H., Agard, P., Schwartz, S., Vidal, O., 2009. Exhumation processes in oceanic and continental subduction contexts: a review. In: Lallemand, S., Funiciello, F. (Eds.), Subduction Zone Geodynamics, pp. 175–205.
Hattori, K.H., Guillot, S., 2003. Volcanic fronts form as a consequence of serpentinite dehydration in the forearc mantle wedge. Geology 31, 525–528.
Hattori, K.H., Guillot, S., 2007. Geochemical character of serpentinites associated with high- to ultrahigh pressure metamorphic rocks in the Alps, Cuba, and the Himalayas: recycling of elements in subduction zones. Geochemistry, Geophysics, Geosystems 8, Q09010.
Hattori, K.H., Hart, S.R., 1997. PGE and Os isotopic signatures for ultramafic rocks from the base of the Talkeetna island arc, Alaska. EOS, Transactions, American Geophysical Union 78 (17), 339.
Hattori, K.H., Guillot, S., Saumur, B.M., Tubrett, M.N., Vidal, O., Morfin, S., 2010a. Corundum-bearing garnet peridotites from northern Dominican Republic: a metamorphic product of an arc cumulate in the Caribbean subduction zone. Lithos 114, 437–450.
Hattori, K.H., Walls, S., Enami, M., Mizukami, T., 2010b. Subduction of mantle wedge peridotites: evidence from the Higashi–Akaishi ultramafic body in the Sanbagawa metamorphic belt. Island Arc 19 (1), 192–207.
Ishii, T., Robinson, P.T., Maekawa, H., Fiske, R., 1992. Petrological studies of peridotites from diapiric serpentinite seamounts in the Izu–Ogasawara–Mariana forearc, Leg 125. In: Fryer, P., Pearce, J.A., Stokking, L.B. (Eds.), Proceedings of the Ocean Drilling Program, Scientific Results, vol. 125. Ocean Drilling Program, College Station, Texas, pp. 445–485.
Kelemen, P.B., 1990. Reaction between ultramafic rock and fractionating basaltic magma I. Phase relations, the origin of calc-alkaline magma series, and the formation of discordant dunite. Journal of Petrology 31, 51–98.
Kelemen, P.B., Shimizu, N., Salters, V.J.M., 1995. Extraction of mid-ocean-ridge basalt from the upwelling mantle by focused flow of melt in dunite channels. Nature 375, 747–753.
Kusky, T.M., Windley, B.F., Zhai, M.G., 2007. Lithospheric thinning in eastern Aisa: contraints, evolution, and tests of models. In: Zhai, M.G., Windley, B.F., Kusky, T.M., Meng, Q.R. (Eds.), Mesozoic sub-continental lithospheric thinning under Eastern Asia: Geological Society, London, Special Publiction, 280, pp. 331–343.
Li, Z.H., Gerya, T.V., 2009. Polyphase formation and exhumation of high- to ultrahigh-pressure rocks in continental subduction zone: numerical modeling and application to the Sulu ultrahigh-pressure terrane in eastern China. Journal of Geophysical Research 114, B09406.
Liu, F.L., Xu, Z., Liou, J.G., 2004. SHRIMP U–Pb ages of ultrahigh-pressure and retrograde metamorphism of gneisses southwestern Sulu terrane, eastern China. Journal of Metamorphic Geology 22 (4), 315–326.
Liu, F.L., Gerdes, A., Zeng, L.S., Xue, H.M., 2008. SHRIMP U–Pb dating, trace elements and the Lu–Hf isotope system of coesite-bearing zircon from amphibolite in the SW Sulu UHP terrane, eastern China. Geochimica et Cosmochimica Acta 72, 2973–3000.
McDonough, W.F., Sun, S.S., 1995. The composition of the Earth. Chemical Geology 120, 223–253.
Meisel, T., Moser, J., 2004. Reference materials for geochemical PGE analysis: new analytical data for Ru, Rh, Pd, Os, Ir, Pt and Re by isotope dilution ICP-MS in 11 geological reference materials. Chemical Geology 208, 319–338.
Melcher, F., Grum, W., Simon, G., Thalhammer, T.V., Stumpfl, E.F., 1997. Petrogenesis of the ophiolitic giant chromite deposits of Kempirsai, Kazakhstan: a study of solid and fluid inclusions in chromite. Journal of Petrology 38 (10), 1419–1458.
Parkinson, I.J., Arculus, R.J., 1999. The redox state of subduction zones: insights from arc-peridotites. Chemical Geology 160, 409–423.
Quick, J.E., 1981. The origin and significance of large, tabular dunite bodies in the Trinity peridotite, northern California. Contributions to Mineralogy and Petrology 78, 413–434.
Rehkämper, M., Halliday, A.N., Alt, J., 1999. Non-chondritic platinum-group elements ratios in oceanic mantle lithosphere: petrogenetic signature of melt percolation? Earth and Planetary Science Letters 127, 65–81.
Righter, K., Campbell, A.J., Humayun, M., Hervig, R.L., 2004. Partitioning of Ru, Rh, Pd, Re, Ir and Au between Cr-bearing spinel, olivine, pyroxene and silicate melts. Geochimica et Cosmochimica Acta 68, 867–880.
Saumur, B.M., Hattori, K., Guillot, S., 2010. Contrasting origins of serpentinites in a subduction complex, northern Dominican Republic. Bulletin of the Geological Society of America 122 (1–2), 292–304.
Sobolev, A.V., Hofmann, A.W., Sobolev, S.V., Nikogosian, I.K., 2005. An olivine-free mantle source of Hawaiian shield basalts. Nature 434, 590–596.
Tang, J., Zheng, Y.F., Wu, Y.B., Gong, B., Zha, X.P., Liu, X.M., 2008. Zircon U–Pb age and geochemical constraints on the tectonic affinity of the Jiaodong terrane in the Sulu orogeny, China. Precambrian Research 161, 389–418.
Tsai, C.H., Liou, J.G., Ernst, W., 2000. Petrological characterization and tectonic significance of retrogressed garnet peridotites, Raobazhai area, North Dabie Complex, east-central China. Journal of Metamorphic Geology 18, 181–192.

Please cite this article as: Xie, Z., et al., Origins of ultramafic rocks in the Sulu Ultrahigh-pressure Terrane, Eastern China, Lithos (2013), http://dx.doi.org/10.1016/j.lithos.2012.12.003

Wallis, S.R., Ishiwatari, A., Hirajima, T., Ye, K., Guo, J., Nakamura, D., Kato, T., Zhai, M., Enami, M., Cong, B., Banno, S., 1997. Occurrence and field relationships of ultrahigh-pressure metagranitoid and coesite eclogite in the Su–Lu terrane, eastern China. Journal of the Geological Society of London 153, 45–54.
Wang, J., Hattori, K.H., Li, J.P., Stern, C., 2008a. Oxidation state of Paleozoic subcontinental lithospheric mantle below the Pali Aike. Lithos 105, 98–110.
Wang, J., Hattori, K.H., Stern, C., 2008b. Metasomatic origin of garnet orthopyroxenites in the subcontinental lithospheric mantle underlying Pali Aike volcanic field, southern South America. Mineralogy and Petrology 94, 243–258.
Wang, J., Hattori, K., Xu, W.L., Yang, Y., Xie, Z.P., Song, Y., 2012a. Origin of ultramafic xenoliths in high-Mg diorites from east-central China based on their oxidation state and abundance of platinum group elements. International Geology Review 54, 1203–1218.
Wang, J., Liu, J.L., Hattori, K., Xu, W.L., Xie, Z.P., Song, Y., 2012b. Behavior of siderophile and chalcophile elements in the subcontinental lithospheric mantle beneath the Changbaishan volcano, NE China. Acta Geologica Sinica 86 (2), 407–422.
Warren, C.L., Baumont, C., Jamieson, R.A., 2008. Formation and exhumation of ultra-high-pressure rocks during continental collision: role of detachment in the subduction channel. Geochemistry, Geophysics, Geosystems 9, Q04019.
Wu, F.Y., Zhao, C.C., Wilde, S.A., Sun, D.Y., 2005. Nd isotopic constrains on the crustal formation of the North China Craton. Journal of Asian Earth Sciences 24, 523–545.
Xu, Y.G., 2001. Thermo-tectonic destruction of the Archean lithospheric keel beneath eastern China: evidence, timing and mechanism. Physics and Chemistry of the Earth, Part A 26, 747–757.
Xu, W.L., Hergt, J.M., Gao, S., Pei, F.P., Wang, W., Yang, D.B., 2008. Interaction of adakitic melt–peridotite: implications for the high-Mg$^{\#}$ signature of Mesozoic adakitic rocks in the eastern North China Craton. Earth and Planetary Science Letters 265, 123–137.
Xu, W.L., Yang, D.B., Gao, S., Pei, F.P., Yu, Y., 2010. Geochemistry of peridotite xenoliths in early Cretaceous high-Mg# diorites from the central orogenic block of the North China Craton: the nature of Mesozoic lithospheric mantle and constraints on lithospheric thinning. Chemical Geology 270, 257–273.
Yang, J.J., 2006. Ca–rich garnet–clinopyroxene rocks at Hujialin in Su–Lu terranc (Eastern China): deeply subducted arc cumulates? Journal of Petrology 47 (5), 965–990.
Yang, J.J., Jahn, B.M., 2000. Deep subduction of mantle-derived garnet peridotites from the Su–Lu UHP metamorphic terrane in China. Journal of Metamorphic Geology 18, 167–180.
Yang, J.S., Xu, Z., Dobrzhinetskaya, L.F., Green, H.W., Pei, X., Shi, R., Wu, C., Wooden, J.L., Zhang, J., Wan, Y., Li, H., 2003. Discovery of metamorphic diamonds in central China: an indication of a >4000-km-long zone of deep subduction resulting from multiple continental collisions. Terra Nova 15, 370–379.
Yao, Y.P., Ye, K., Liu, J.B., Cong, B.L., Wang, Q.C., 2000. A transitional eclogite to high pressure granulite–facies overprint on coesite–eclogite at Taohang in the Sulu ultrahigh-pressure terrane, eastern China. Lithos 52, 109–120.
Ye, K., Cong, B.L., Ye, D.N., 2000. The possible subduction of continental material to depths greater than 200 km. Nature 407, 734–736.
Ye, K., Song, Y.R., Chen, Y., Xu, H.J., Liu, J.B., Sun, M., 2009. Multistage metamorphism of orogenic garnet-lherzolite from Zhimafang, Sulu UHP terrane, E. China: implications for mantle wedge convection during progressive oceanic and continental subduction. Lithos 109, 155–175.
Ying, J.F., Zhang, H.F., Kita, N., Morishita, Y., Shimoda, G., 2006. Nature and evolution of Late Cretaceous lithospheric mantle beneath the eastern North China Craton: constraints from petrology and geochemistry of peridotitic xenoliths from Jünan, Shandong Province, China. Earth and Planetary Science Letters 244, 622–638.
Yoshida, D., Hirajima, T., Ishiwatari, A., 2004. Pressure–temperature path recorded in the Yangkou garnet peridotite, in Su–Lu ultrahigh-pressure metamorphic belt, eastern China. Journal of Petrology 45 (6), 1125–1145.
Zhang, R.Y., Liou, J.G., 2003. Clinopyroxenite from the Sulu ultrahigh-pressure terrane, eastern China: origin and evolution of garnet exsolution in clinopyroxene. American Mineralogist 88, 1591–1600.
Zhang, R.Y., Liou, J.G., Yang, J.S., Yui, T.F., 2000. Petrochemical constraints for dual origin of garnet peridotites from the Dabie–Sulu UHP terrane, eastern-central China. Journal of Metamorphic Geology 18, 149–166.
Zhang, R.Y., Yang, J.S., Wooden, J.L., Liou, J.G., Li, T.F., 2005. U–Pb SHRIMP geochronology of zircon in garnet peridotite from the Sulu UHP terrane, China: implications for mantle metasomatism and subduction-zone UHP metamorphism. Earth and Planetary Science Letters 237, 729–743.
Zhang, R.Y., Pan, Y.M., Yang, Y.H., Li, T.F., Liou, J.G., Yang, J.S., 2008. Chemical composition and ultrahigh-P metamorphism of garnet peridotites from the Sulu UHP terrane, China: investigation of major, trace elements and Hf isotopes of minerals. Chemical Geology 255, 250–264.
Zhang, R.Y., Liou, J.G., Ernst, W.G., 2009. The Dabie–Sulu continental collision zone: a comprehensive review. Gondwana Research 16, 1–26.
Zhang, R.Y., Jahn, B.M., Liou, J.G., Yang, J.S., Chiu, H.-Y., Chuang, S.-L., Li, T.-F., Lo, C.-H., 2010. Origin and tectonic implication of an UHP metamorphic mafic–ultramafic complex from the Sulu UHP terrane, eastern China: evidence from petrological and geochemical studies of CCSD–Main Hole core samples. Chemical Geology 276, 69–87.
Zhao, G.C., Wilde, S.A., Cawood, P.A., Sun, M., 2001. Archean blocks and their boundaries in the North China Craton: lithological, geochemical, structural and P–T path constraints and tectonic evolution. Precambrian Research 107, 45–73.
Zheng, J.P., Lu, F.X., 1999. Mantle xenoliths from kimberlites, Shandong and Liaoning: Paleozoic mantle character and its heterogeneity. Acta Petrologica Sinica 15, 65–74 (in Chinese with English Abst.).
Zheng, J.P., O'Reilly, S.Y., Griffin, W.L., Lu, F.X., Zhang, M., Pearson, N.J., 2001. Relics of refractory mantle beneath the eastern North China block: significance for lithosphere evolution. Lithos 57, 43–66.
Zheng, Y.F., Wu, Y.B., Chen, F.K., Gong, B., Li, L., Zhao, Z.F., 2004. Zircon U–Pb and oxygen isotope evidence for a large-scale ^{18}O depletion event in igneous rocks during the Neoproterozoic. Geochimica et Cosmochimica Acta 68, 4145–4165.
Zheng, J.P., Zhang, R.Y., Griffin, W.L., Liou, J.G., O'Reilly, S.Y., 2005a. Heterogeneous and metasomatized mantle recorded by trace elements in minerals of the Donghai garnet peridotites, Sulu UHP terrane, China. Chemical Geology 221, 243–259.
Zheng, J.P., Sun, M., Zhou, M.F., Robinson, P., 2005b. Trace elemental and PGE geochemical constraints of Mesozoic and Cenozoic peridotitic xenoliths on lithospheric evolution of the North China Craton. Geochimica et Cosmochimica Acta 69 (13), 3401–3418.
Zheng, J.P., Griffin, W.L., O'Reilly, S.Y., Yang, J.S., Li, T.F., Zhang, M., Zhang, R.Y., Liou, J.G., 2006. Mineral chemistry of peridotites from Paleozoic, Mesozoic and Cenozoic Lithosphere: constraints on mantle evolution beneath Eastern China. Journal of Petrology 47, 2233–2256.
Zheng, J.P., Griffin, W.L., O'Reilly, O.Y., Yu, C.M., Zhang, H.F., 2007. Mechanism and timing of lithospheric modification and replacement beneath the eastern North China Craton: peridotitic xenoliths from the 100 Ma Fuxin basalts and a regional synthesis. Geochimica et Cosmochimica Acta 71, 5203–5225.
Zheng, J.P., Sun, M., Griffin, W.L., Zhou, M.F., Zhao, G.C., Robinson, P., Tang, H.Y., Zhang, Z.H., 2008. Age and geochemistry of contrasting peridotite types in the Dabie UHP belt, eastern China: petrogenetic and geodynamic implications. Chemical Geology 247, 282–304.
Zhu, R.X., Yang, J.H., Wu, F.Y., 2012. Timing of destruction of the North China Craton. Lithos 149, 51–60.

Please cite this article as: Xie, Z., et al., Origins of ultramafic rocks in the Sulu Ultrahigh-pressure Terrane, Eastern China, Lithos (2013), http://dx.doi.org/10.1016/j.lithos.2012.12.003